J Math Chem (2014) 52:368–397
DOI 10.1007/s10910-013-0268-y

ORIGINAL PAPER

A new adaptive mutation simulated annealing algorithm: application to the study of pure and mixed Pt–Pd clusters

Shyamal Kumar Biring · Rahul Sharma · Pinaki Chaudhury

Received: 3 July 2013 / Accepted: 30 September 2013 / Published online: 9 October 2013

Abstract In this article we would like to propose a modified simulated annealing procedure termed as adaptive mutation simulated annealing. In this, the parameters within the optimization scheme is dynamically updated keeping in view the requirements of the parameter values needed for efficient and unequivocal identification of the global minimum in a really rugged multiple minima surface. We apply this procedure to the problem of finding out the global minimum structures of pure Platinum and Palladium clusters as well as the mixed *Pt–Pd* ones (for cluster sizes upto 60), where the interactions among the constituents of the cluster are defined by the many body empirical Gupta potential. Once the structures are obtained, we try to find out the sizes for which the clusters possess greater stability. These so called magic numbers are compared with existing literature values. To test the efficiency of the proposed procedure we compare the results with conventional simulated annealing. We also analyse in detail and calculate various statistical properties and their evolution during the adaptive mutation simulated annealing run. This in-depth analysis gives an insight into why the current procedure outperforms the conventional simulated annealing.

Keywords Simulated annealing · Adaptive simulated annealing · Atomic cluster · Bimetallic cluster · Platinum–Palladium cluster

S. K. Biring · P. Chaudhury (✉)
Department of Chemistry, University of Calcutta, 92 A.P.C. Road,
Kolkata 700009, West Bengal, India
e-mail: pinakc@rediffmail.com

R. Sharma
Department of Chemistry, St. Xaviers' College, 30 Mother Teresa Sarani,
Kolkata 700016, West Bengal, India

1 Introduction

Determination of geometrical structures of clusters is of fundamental importance as it affects all aspects of the chemical and physical behaviour of such systems. A large amount of literature has focused on the study of nano-clusters due to the variety of their technological uses [1–12].

There are two aspects to the determination of minimum energy structures [13–21], which are actually considered to be chemically important. It must be emphasised here that the lowest energy structure or the global minimum is of paramount importance but the low lying local energy structures have their importance too. In a real experimental situation, if the energy barrier between the global and the low lying local structures are not very much, the structure which can be sensed experimentally at a finite temperature and in a given finite time is generally an average over all these near energy conformations. Firstly, the calculation of the energy associated with a particular geometric configuration can be determined at an ab initio level of calculation or some phenomenological potential [22–31] can be used to do the same at a lower computational cost but the structures computed using these empirical potentials are approximations to the ones obtained using calculations at some quantum chemical level of theory. However, it must also be stressed that if the empirical potential is of high quality i.e. is able to essentially take into account all the major inter atomic interactions then the structures obtained as critical points on this empirical potential energy surface is extremely close to the ones obtained using quantum chemical calculations [32,33]. So, though the use of empirical potentials generate approximate structures, the degree of approximation can be substantially reduced by improving the quality of the empirical potential.

Secondly, the task of structure evaluation involves a process of optimization of the geometrical parameters. On a potential energy hypersurface stable structures are the ones for which the gradient norm is zero. The significance of zero gradient norm is that it implies a point on the hypersurface where there are no unbalanced forces acting on the particles forming the chemical entity. Only if there are no unbalanced forces, does a real equilibrium geometry is generated. The theoretical estimation or determination of such structure is a non-trivial task in itself and in most applications, most of deterministic techniques fail if the search is on a surface which is extremely rugged and supports multiple minima of varying depths. Deterministic techniques are gradient based and these methods if used, always leads to the finding out of the minimum which is nearest to the starting point from which the search was initiated. Hence the objective of finding the global minimum from a myriad of possibilities (for multi minimal surfaces) becomes an onerous one. The only way out of this difficulty is to perform multiple optimization procedures with different starting point and check the final convergence, and from the output of all these runs select the best result obtained so far. Even after these multiple runs the task of finding the global minimum might remain elusive. So we can conclude that for extremely rugged surfaces using deterministic techniques is a poor choice both in terms of the quality of results obtained as well as the computational cost. The way out is to switch over to non-deterministic (stochastic) techniques which uses concepts of random walk and Markov chains to surmount energy barriers separating different energy conforma-

tions and ultimately unequivocally find out the global minimum. In a nutshell, to design robust and high performing optimization processes the basic philosophy of using the gradient as a dictator of the search on a hypersurface must be done away with.

There has been a plethora of techniques that are in vogue which perform a more global search on such potential energy surfaces like simulated annealing (SA) [34–44], Genetic Algorithms [20,45–52], Basin Hopping [53,54] etc. But all of them at varied levels entail high computational cost and/or suffer from the problem of premature convergence. There already exists a huge amount of literature which even after highlighting the power of these methods touch upon the reality of the above mentioned problems [48]. There have also been attempts to address these issues and find probable way out by making necessary modifications to correct these problems. However the success of these attempts have been varied and most authors have pointed to the fact that a particular modification at the algorithmic level generally does not produce an omnipotent search strategy.

In the present communication we take up the Simulated Annealing method that has been applied to a large number of problems over a long period of time. SA is based on the conventional metallurgical process of annealing. In this method initially the system is allowed to equilibriate at a high 'temperature' and is 'cooled' gradually leading to the thermodynamically most stable state (global minimum) of the system. The practical application of SA suffers from 'freezing out' or premature convergence both due to a finite number of steps spent on trying to equilibriate the system at a particular temperature and the rather fast cooling of the system. To overcome this deficiency a lot of work has been done in the past and our present attempt is at overcoming this premature convergence problem using our adaptive mutation simulated annealing (AMSA) without undue enhancement of the computational cost. We have chosen the determination of the global minimum structures, as well as a few low lying ones, of Platinum, Palladium pure clusters as well as Pt–Pd mixed clusters, for cluster sizes from 2 to 60, where the structures are evaluated by assuming the interaction between the atoms being modelled by the suitably parametrised Gupta Potential.

2 Methodology

2.1 Gupta potential

Usually for large clusters of atoms since large area of configuration space are to be searched so ab-initio calculations are infeasible starting with a random guess for the putative structure. Thus much interest has been shown in developing empirical atomistic potentials to allow relatively rapid searching of such space that lead to good guess structures that can be further refined using some level of ab-initio calculation. To that end, many body-empirical potentials [22–31], such as the Gupta Potential [27,28] has been derived by fitting experimental data to values calculated using a potential of an assumed functional form. Gupta Potential is usually used to describe the inter-atomic bonding in transition and noble metal clusters. This potential function is obtained

Table 1 Gupta potential parameters for Pt–Pd clusters [20]

	Pt–Pt	Pd–Pd	Pt–Pd*(I)*
A/eV	0.2975	0.1746	0.23
ζ/eV	2.695	1.718	2.2
p	10.612	10.867	10.74
q	4.004	3.742	3.87
r_0/Å	2.7747	2.7485	2.76

from a tight-bonding second moment approximation of the density of states for the 'd' electrons and comprises an attractive many body (V^m) term and a repulsive pair (V^r) term, summed over all N atoms:

$$V_{clus} = \sum_{i}^{N} \left\{ V^r(i) - V^m(i) \right\} \tag{2.1}$$

where $V^r(i)$ and $V^m(i)$ are defined as:

$$V^r(i) = \sum_{j \neq i}^{N} A(a,b) exp \left\{ -p(a,b) \left(\frac{r_{ij}}{r_0(a,b)} - 1 \right) \right\} \tag{2.2}$$

and

$$V^m(i) = \left[\sum_{j \neq i}^{N} \zeta^2(a,b) exp \left\{ -2q(a,b) \left(\frac{r_{ij}}{r_0(a,b)} - 1 \right) \right\} \right]^{\frac{1}{2}} \tag{2.3}$$

In Eqs. 2.2 and 2.3, r_{ij} is the distance between atoms i and j in the cluster, and A, r_0, ζ, p, q are fitted to experimental values of the cohesive energy, lattice parameters and independent elastic constants for the reference crystal structure at 0 K.

The Gupta Potential parameters, for *Pt–Pd* alloy clusters, take different values depending on the nature of interaction (*Pt–Pt*, *Pd*–Pd and *Pt–Pd* type). The *Pt–Pt* and *Pd–Pd* parameters were derived by Cleri and Rosato [28] by fitting to the pure metals, whereas *Pt–Pd* parameters were derived by taking the averages of the *Pt–Pt* and *Pd–Pd* parameters and these are listed in Table 1.

Due to low enthalpy of formation, the *Pt–Pd* alloys are solid solution for all composition. Parameters p and q in the Gupta Potential are taken to be as measures of the ranges of the repulsive and attractive interaction respectively, where 'a' and 'b' are the atomic labels for ith and jth atom. Thus with the increasing inter atomic separation the pair or the many-body energy contributions die off. From the parameter table it is clear that larger 'A' value for Pt means that the pair term is more repulsive for Pt than Pd but from the angle of attractive many body potential Pd has a smaller hopping integral (ζ) than Pt, showing the smaller cohesive energy of bulk Pd compared to Pt. So the nature of pair and many body potential energy terms are important in determining the type and stabilities of different cluster systems.

2.2 Geometry optimization

The method we have used to search for the minimum energy cluster structure is based on thermal fluctuation based stochastic optimizer, SA, which is a global search technique. It is based on the Metropolis Monte Carlo Algorithm [55] which was modified as a numerical optimization problem by Kirkpatrick et al. [34], Cerny [36] and Pincus [37], independently. It was generalized for optimization of functions of continuous variables by Vanderbilt and Louie [38]. The ability of SA to jump over local minima to converge to the global one was claimed and has been proven analytically [56].

2.2.1 The simulated annealing scheme

The potential energy surfaces of atomic clusters are some multi-minimal hypersurfaces with a number of local minima. SA can therefore overcome any local energy barrier which needs to be crossed en-route to the lower minimum.

The working principle of SA starts from defining the variables that need to be optimized (the geometrical parameters $\{x_i\}_{i=1,\ldots,3N}$ for a cluster of N atoms, in this case). Then a corresponding objective function (F) or the cost function, which needs to be minimized, determined with respect to a particular geometrical parameter set, is defined by:

$$F = U\{x\} \tag{2.4}$$

where 'U' is a computed energy (using some energy function) of a particular geometrical parameter value set $\{x\}$.

We start a particular SA run by making a random guess for the initial geometrical parameter set $\left\{x^{(current)}\right\}$, and compute the associated energy ($U^{(current)}$) and the objective function value or cost ($F^{(current)}$).

The system is considered to be maintained at an artificially defined 'temperature' (T_{in}).

A new geometrical parameter set $\{x^{new}\}$ is generated from the previous existing one ($\left\{x^{current}\right\}$) usually via introduction of a random change in one of the parameter values, but what we have used is a multiple point arithmetic mutation scheme where each and every parameter has a finite probability of undergoing change. Multiple point arithmetic mutation is implemented by defining a mutation probability p_m. For each variable, a probability check is performed ($p_m > r$, where r is a random number) which when found to be true leads to an arithmetic mutation of that variable given as:

$$x_k^{new} = x_k^{current} \pm r f_m \tag{2.5}$$

where r is another random number and f_m is a user defined mutation intensity that defines the amplitude of mutation. Here we ensure that there must be change in at least one variable.

The corresponding energy U^{new} and the cost F^{new} are computed and we determine the difference in costs of the current and new parameter set given as:

$$\Delta F = F(\{x^{new}\}) - F(\{x^{current}\}) \tag{2.6}$$

If ΔF is negative the move is accepted i.e. we set:

$$\{x^{current}\} = \{x^{new}\} \tag{2.7}$$

If not the move is subjected to the Metropolis test according to the following sampling probability (P), which is given by:

$$P = e^{\frac{-\Delta F}{KT}} \tag{2.8}$$

where T is SA temperature. The quantity 'P' scales between 0 and 1. Once 'P' is evaluated, a random number (R) between 0 and 1 is called. If $P > R$, the move is accepted, if not the move is rejected leading to the positional co-ordinates of the atomic cluster remaining unchanged. It is clear that if T is high, 'P' will be close to 1, and most move will qualify the Metropolis test. The SA temperature T can be thought of as a parameter which controls the thermal fluctuations. The central idea is that during the initial stages of search T is kept high so that the search space is sampled at greater lengths till the correct direction is achieved and if a search is trapped in a local attractive basin, the high temperature T helps to jump out of it to search a more deeper minimum. But in the latter stages of the search a low T is perfectly all right as the need for crossing local energy barriers do not arise. Hence T in a typical SA run is kept high to start with, the mutation and metropolis test is applied multiple times to allow the system to 'equilibriate' with the temperature 'T' or allowed to sample for a large number of steps n_{Metrop} (hoping that equilibrium is achieved), and then the temperature is slowly decreased, following a schedule called cooling schedule and in the limit of $T \rightarrow 0$ the right solution is hopefully found out. Here we have used the cooling schedule given by:

$$T_{new} = T_{old} * \lambda_{cool} \tag{2.9}$$

where λ_{cool} is a user defined parameter ($0.0 < \lambda_{cool} < 1.0$).

There is a possibility that final set obtained after such a cooling schedule might not be the global minimum (an effect of premature convergence), principally caused due to a cooling schedule which, for practical purposes, is not performed infinitesimally slowly. So we might need to re-anneal the system i.e. we reset the temperature 'T' to a high value (but less than 'T_{in}') and repeat the process for a number of times.

2.2.2 Adaptive arithmetic mutation

It was proven that global minima can be achieved if the initial temperature is taken high enough and the cooling schedule is extremely slow. Many variants of annealing have been reported [57–59] but they usually require values for parameters that are problem specific moreover the slowness in attaining the result remains. Any attempt at better computational efficiency leads to some decrease in the probability of finding out good quality results.

In order to enhance the exploration and the convergence properties of the SA scheme we have applied an adaptive mutation scheme where the mutation probability (p_m) as well as mutation intensity (f_m) {defined below} are modified during the search process at a particular temperature based upon the fraction of mutations (r_m) that pass the Metropolis criterion (n_{accept}) to the total number of samples done ($n_{samples}$). A related scheme has been successfully applied in the case of Genetic Algorithm [60] and a unique Random Mutation Hill Climbing [61] method for optimization in a continuous variable space, previously.

In this particular scheme, after every successful Metropolis step, n_{accept} is updated by a unit value. On completion of n_{sample} number of steps at a particular temperature, we compute r_m as:

$$r_m = \frac{n_{accept}}{n_{samples}} \tag{2.10}$$

where $0.0 \leq r_m \leq 1.0$, $n_{samples}$ is actually taken as a fraction of the total number of samples at a particular temperature (n_{Metrop}) as $n_{samples} = n_{Metrop}/i_{samples}$ where $i_{samples}$ is a small integer.

If the value of r_m remains within the user defined range of $[r_m^{min}, r_m^{max}]$ ($0.0 < r_m^{min}, r_m^{max} < 1.0$ and $r_m^{min} < r_m^{max}$), then neither p_m nor f_m is changed.

A value of r_m greater than r_m^{max} implies that a large fraction of Metropolis sampling is successful and we can allow a greater exploration of the search space; thus we increase the value of p_m or f_m as:

$$y = y * (2.0 - \Delta_y * r) \tag{2.11}$$

where $y = p_m$ or f_m, Δ_y is a user defined parameter from the range [0.0, 1.0], r is a random number from the range [0.0, 1.0].

If the value of r_m turns out to be less than r_m^{min}, it implies a non-optimal search so we decrease the value of p_m or f_m as:

$$y = y * \Delta_y * r \tag{2.12}$$

Throughout, p_m and f_m have an equal probability of undergoing change.

Then we reset n_{accept} to a value of zero and continue the sampling procedure.

Using the adaptive mutation scheme we hope to enhance the exploratory properties of the search scheme and expect a better convergence to the global minimum with a greater deal of certainty for each run.

There exist several cooling schedules in literature [64–67], We have used an geometric cooling schedule followed by reheating to a higher temperature after the completion of each cooling schedule. Similar schemes have been used previously [62], even allowing for reheating adaptively [58,67].

We have compared our results with that of the standard form of SA and no comparison is made with the highly celebrated Adaptive Simulated Annealing of Ingber [62,63] since the experiments we had with their available code requires fine tuning of the various program parameters otherwise the comparison stands redundant.

2.3 Features of the method using adaptive SA

The adaptive SA runs always converge to the global minimum for any size cluster, while a simple conventional SA might not. The probable reason might be that during an adaptive SA run, as the parameters (temperature, mutation amplitude, mutation probability) are rescaled to certain appropriate values at periodic intervals, the changes are such that the simulation run picks up the right parameters which ultimately drives it to the global minimum. In a conventional SA run, the parameter set is fixed in a given run and some times fail to locate the global minimum unequivocally. So multiple run might be needed which ultimately shoots up the computational cost. So an adaptive SA is efficient both from the view points of efficiency as well as efficacy.

How far is the rescaling of parameters successful in inducing positive changes in the search geometry?

It is evident from the results obtained (discussed in the following section) that as the temperature is rescaled, the search parameters are also logically rescaled and some associated features also show changes in behaviour and this changing behaviour roughly mirrors the pattern of change of the temperature. At a rescaled high temperature, the fluctuation in energy also increases, which then gradually decreases with the decrease of temperature. The increased energy fluctuation starts instantly as the temperature is readjusted to a high value. However, our ultimate goal is to find the lowest energy structure. If we call E_{best} as the energy of the lowest energy structure so far obtained, then it is important to see if the rescaling of the simulation parameters have an effect on it. from the plot of the E_{best} against the number of SA steps, we see that a better E_{best} might not be found out as soon as the temperature and the associated parameters are rescaled but once the change is made better state is found out if the simulation is allowed to proceed for a limited number of steps. So in adaptive SA, the plateau nature of the energy profile, (where no better energy state is found out over a large number of steps) is relatively short compared to a conventional SA run. So, we can categorically comment that the adaptive SA can cause convergence at faster rates compared to the conventional version.

3 Results and discussion

3.1 Analysis of adaptive mutation simulated annealing (AMSA)

In this section we analyse in detail the important features of AMSA and how does it compare vis-a-vis a fixed parameter Simulated Annealing. Figures 1, 2, 3, and 4 show the evolution of various parameter related to the AMSA run where the run has been carried out over different number of Metropolis steps at a particular temperature. In Fig. 1 the simulation run is over $500 * 3N$ steps where '$3N$' is the total number of co-ordinates to be optimized. Figure 1a shows the temperatures at various steps (periodical reheating is done with a parameter $\lambda_{reheat} = 0.9$) and the decrease in temperature is done to multiply the present temperature with $\lambda_{cool} = 0.8$). Figure 1b shows the variation $E_{best} - E_{globalbest}$, where E_{best} is the lowest value of energy obtained at a given temperature and $E_{globalbest}$ is the final target value in energy. It is

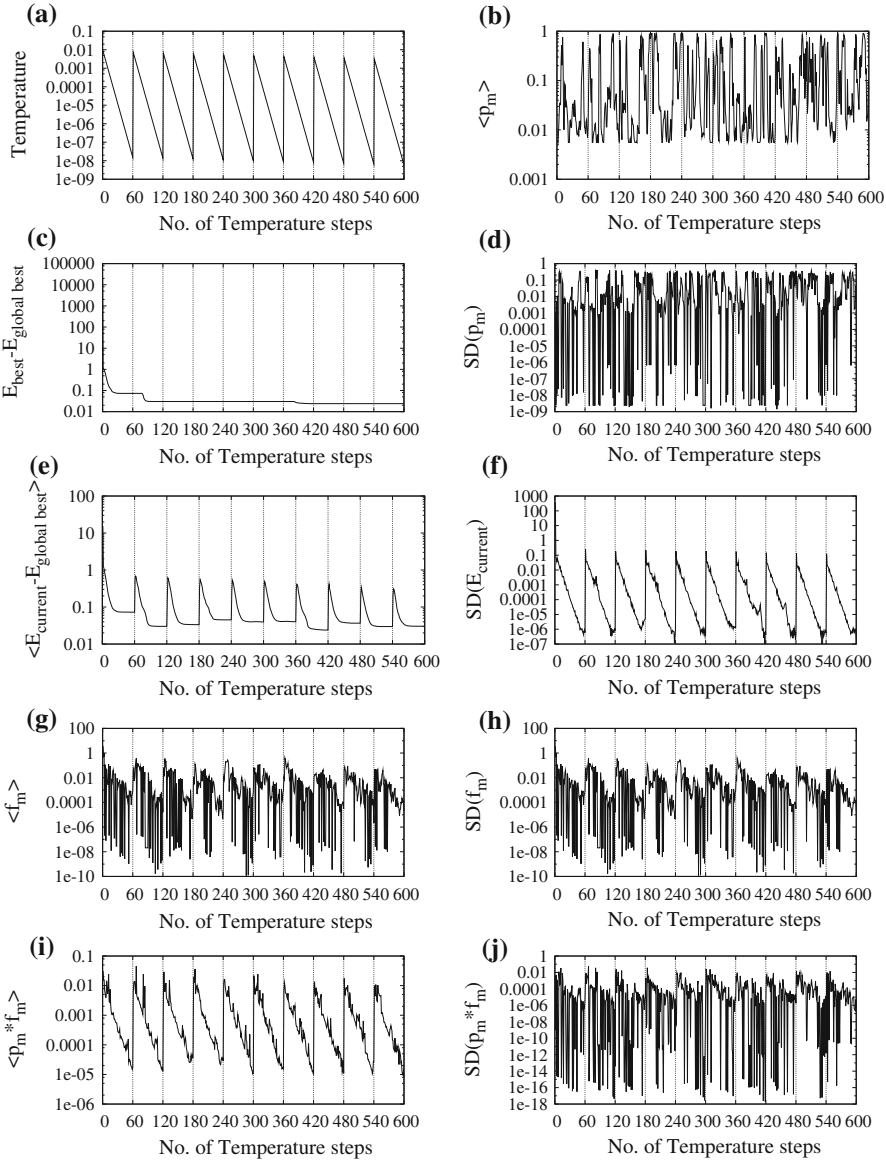

Fig. 1 For run with $n_{Metrop} = 500 * 3n$, adaptive p_m and f_m, $\lambda_{reheat} = 0.9$, $\lambda_{cool} = 0.8$

seen that the best value of $E_{best} - E_{globalbest}$ obtained is around 0.01 (which is some distance away from full convergence). Figure 1c shows the average energy obtained at a given temperature designated as $\langle E_{current} \rangle$ (here all energy values have been scaled with respect to the known global best energy where the values have been rounded off to 7 decimal places, and logarithmic scaling has been used throughout) with the number of Metropolis steps at a particular temperature. The plot roughly mirrors the variation in temperature with the periodic peaks being observed at the same number

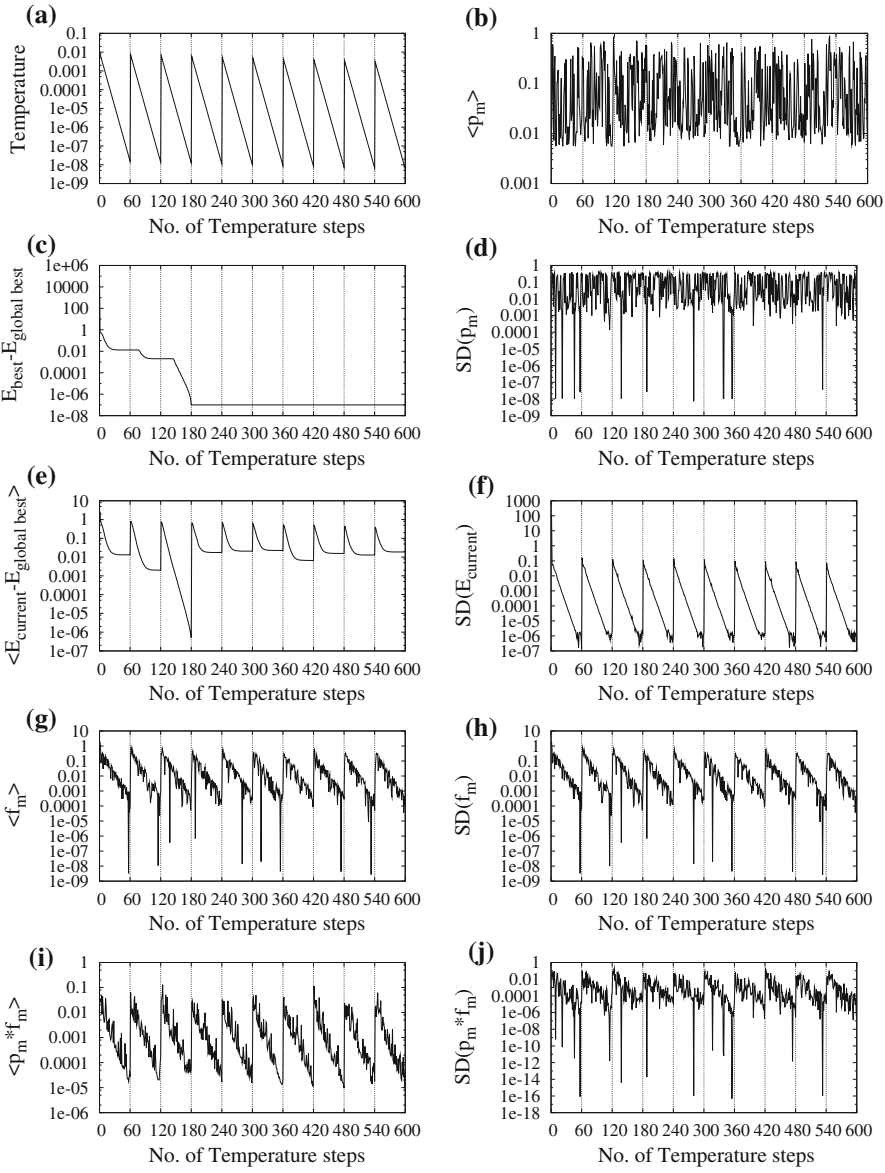

Fig. 2 For standard run with $n_{Metrop} = 1{,}000 * 3n$, adaptive p_m and f_m, $\lambda_{reheat} = 0.9$, $\lambda_{cool} = 0.8$

steps. Figure 1d–f show the variation of the average mutation amplitude ($\langle f_m \rangle$), the product of mutation amplitude and mutation probability ($\langle p_m * f_m \rangle$) and the mutation probability ($\langle p_m \rangle$) itself. It must be noted that only in Fig. 1e which is $\langle p_m * f_m \rangle$ versus no. of temperature steps, does the profile roughly mirrors the temperature variation profile of Fig. 1a. Figure 1g–j shows the variation of the standard deviations of the quantities p_m, $E_{current}$, f_m and $P_m * f_m$ with the no. of the steps. Only in Fig. 1h,

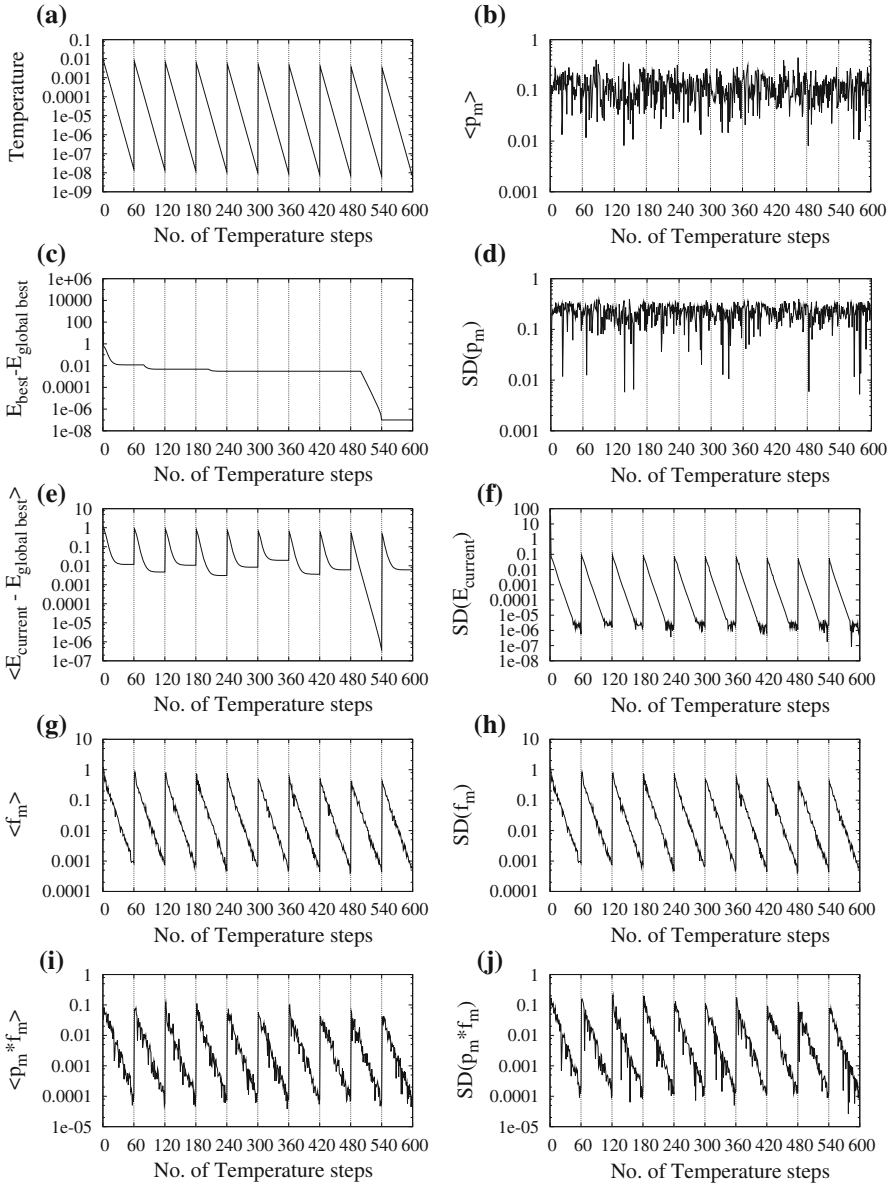

Fig. 3 For run with $n_{Metrop} = 2{,}000 * 3n$, adaptive p_m and f_m, $\lambda_{reheat} = 0.9$, $\lambda_{cool} = 0.8$

which is $SD(E_{current})$ does a close correspondence with the temperature variation noticed.

Figures 2a–j show similar profiles when the simulation has been carried out over 1,000*3N generation or steps. The features that are worth noticing is that the $E_{best} - E_{globalbest}$ Fig. 2b reaches a low value of nearly 10^{-6}, which means that the final low energy structure obtained is much better compared to the earlier case. Figure 2c

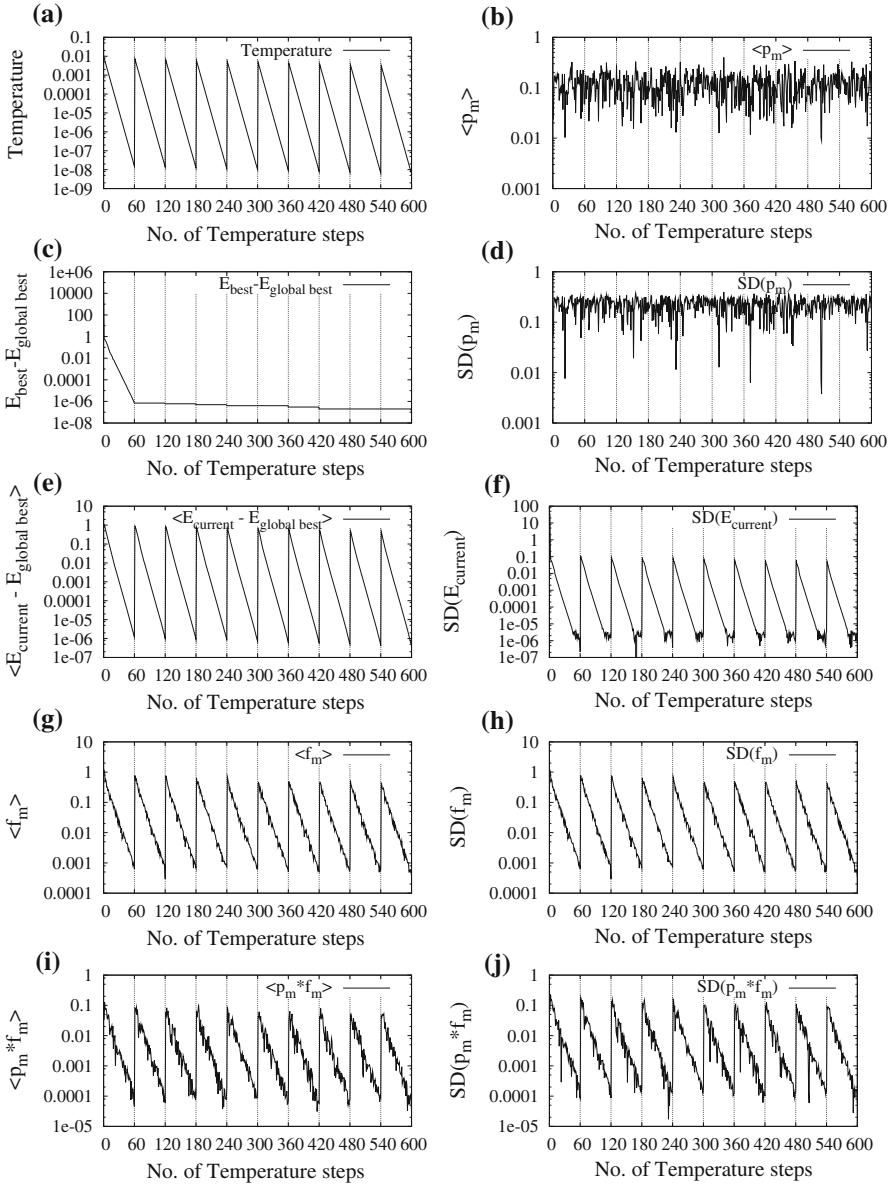

Fig. 4 For run with $n_{Metrop} = 2{,}000 * 3n$, adaptive p_m and f_m, $\{x_{current}\}$ reset to $\{x_{best}\}$ after run at a particular T, $\lambda_{reheat} = 0.9$, $\lambda_{cool} = 0.8$

which the variation of $\langle E_{current} \rangle$ also shows very important features. At around 180 temperature steps a low value of 10^{-6} is reached and on subsequent upgrading of temperature, various plateau like regions are obtained which are of higher $\langle E_{current} \rangle$. These higher plateau like regions signify the achievement of local minima. So in a particular AMSA run several local structures in addition to the global can in principle

be isolated. The other figures in general mirror those for the first run with $500 * 3N$ steps except that move smooth features with less oscillations are observed in general. However the $\langle p_m \rangle$ still shows large fluctuations (Fig. 2f).

Figures 3a–j show similar profiles when the simulation has been carried for $2{,}000 * 3N$ steps. In general the profiles are smoother with the $E_{best} - E_{globalbest}$ reaching a low values of nearly 10^{-6} (Fig. 3c). The most noteworthy feature is the decrease in fluctuations in $\langle p_m \rangle$ and $SD(p_m)$, with an approach towards a value of 0.1 for the $\langle p_m \rangle$. This magnitude of mutation probability, we believe is the optimal choice for the present problem being looked into.

Till now in the figures being discussed, whenever the temperature was readjusted to a higher value periodically, the structure with the best energy obtained in the immediate previous temperature step was used as the starting point for new exploration. However a parallel strategy would be to use the best energy obtained so far among all the previous temperature steps, rather than the immediate previous best. This is done in Fig. 4a–j. The only noteworthy feature to be reported is that this strategy does not locate various local minima in addition to the global, but the achievement of global minima is guaranteed like the earlier ones. The optimum value of $p_m = 0.1$ can also be guessed from these runs.

We now look into the profiles of runs with fixed parameters in an SA, i.e. where the p_m and f_m were not allowed to vary. Figure 5a–f show the profiles for the variations

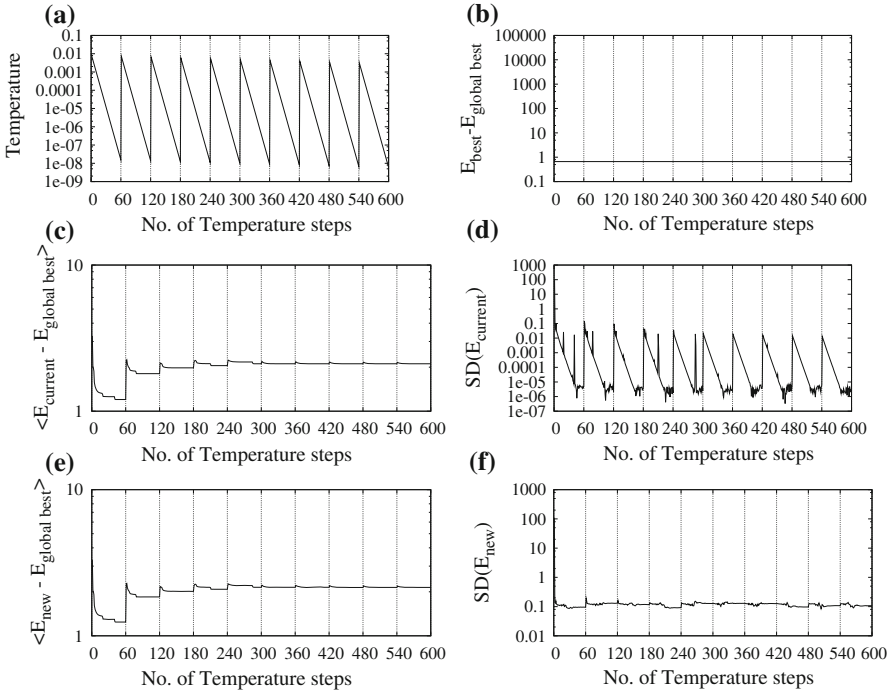

Fig. 5 For run with fixed parameters ($f_m = 1.0$, single point mutation, $\lambda_{reheat} = 0.9$, $\lambda_{cool} = 0.8$) and with $n_{Metrop} = 2{,}000 * 3n$

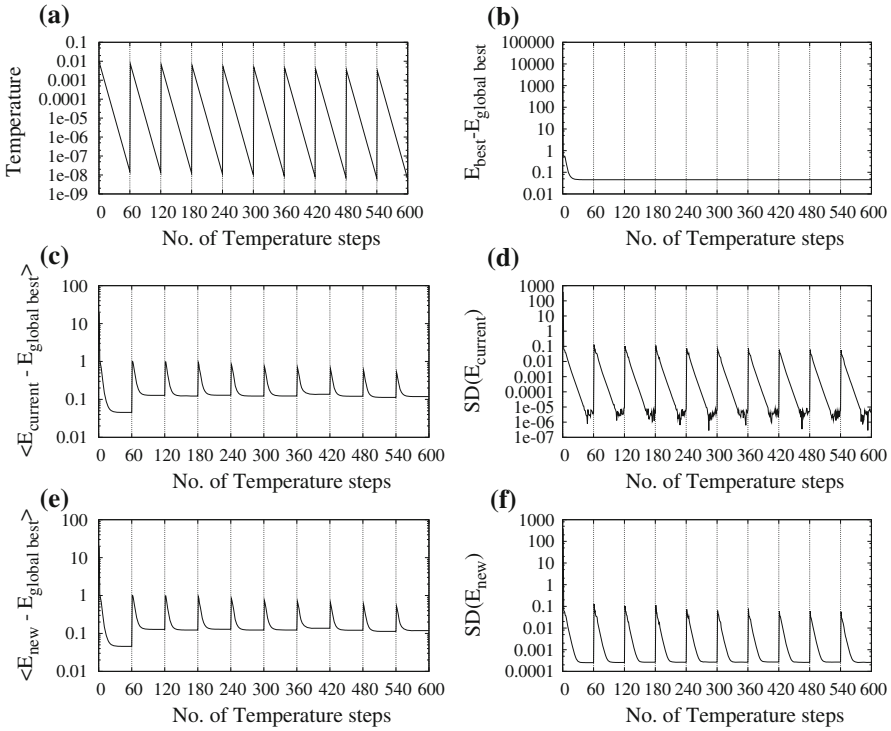

Fig. 6 For run with fixed parameters ($f_m = 0.1$, single point mutation, $\lambda_{reheat} = 0.9$, $\lambda_{cool} = 0.8$) and with $n_{Metrop} = 2{,}000 * 3n$

of the relevant parameters. The number of steps or generations over which the run was carried out is $2{,}000 * 3N$, i.e. the same number of steps for which we got the best results with AMSA. The point to be noted is that the plot of $E_{best} - E_{globalbest}$ (Fig. 5b) converges to a value of around 1, which means that this run has shown extremely poor convergence. The f_m value for this run was kept at 1.0. In Fig. 6a–f similar profiles are shown but with a $f_m = 0.1$ and this leads to a better value for $E_{best} - E_{globalbest}$ (0.1), but this is still far away from an acceptable good minimum. In Fig. 7a–f, f_m to 0.01 and this leads to a some what better value to around 0.001 but still this is no way near to around 10^{-6} obtained with AMSA. It must also be noted tha in the AMSA runs, not only lower energy structures were obtained but they were seen to appear at much lesser number of temperature steps. So we can conclude that AMSA is better than a fixed parameter SA both in terms of efficacy as well as efficiency. The efficiency of Boltzmann Annealing scheme [68] mimics that for the one obtained for the case of Fig. 7. Having established the relative superiority of AMSA over fixed point SA, we further proceeded to see the effects of λ_{reheat} and λ_{cool} on a AMSA run. Figures 8, 9, and 10 show the variation of different parameters and their standard deviations, keeping $\lambda_{cool} = 0.8$ for all of them and $\lambda_{anneal} = 0.9$, 0.8 and 0.7 respectively. What we observe is that a $\lambda_{reheat} = 0.9$ perform much better with the $E_{best} - E_{globalbest}$ reaching a steady low value of 10^{-6} and a very quick initial decrease by about 60

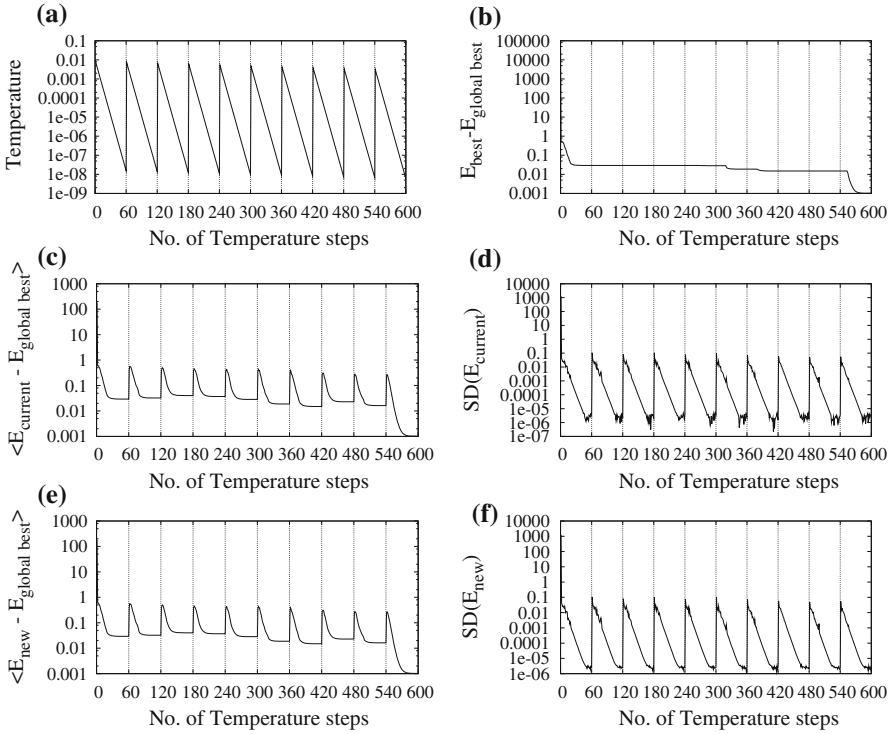

Fig. 7 For run with fixed parameters ($f_m = 0.01$, single point mutation, $\lambda_{reheat} = 0.9$, $\lambda_{cool} = 0.8$) and with $n_{Metrop} = 2{,}000 * 3n$

temperature steps. Figures 11, 12 and 13 reports results from AMSA runs keeping $\lambda_{reheat} = 0.9$ and λ_{cool} being 0.7, 0.6 and 0.5 respectively. It is observed that a $\lambda_{cool} = 0.5$ (Fig. 13) show poorest convergence with $E_{best} - E_{globalbest}$ being lowered to a value of only 0.1. We can thus conclude that both a high value of λ_{reheat} and λ_{cool} can lead to better convergence in AMSA runs. Our aim in this communication has been to devise a scheme that can throw up the best so far known result with greater regularity. To that end we observe that our AMSA with $2,000 * 3N$ number of Metropolis steps per temperature has shown an efficiency of 100 % for the pure Pt, pure Pd and Pt–Pd mixed clusters of various sizes discussed in the next section. The AMSA scheme with $1,000 * 3N$ number of Metropolis steps has an efficiency of 100 % for all pure clusters and small sized ($n \leq 20$) mixed clusters whereas for mixed cluster of larger sizes ($21 \leq n \leq 30$) we observe an efficiency of ∼90 %. The performance of the two methods, AMSA and standard SA, is summarized in Table 2.

3.2 Application of AMSA

The SA parameters that have been used here are given in Table 3.

Calculation for optimization were carried out for selected Pt, Pd and Pt–Pd clusters with 2–60 atoms. For this purpose using SA method with the help of empirical

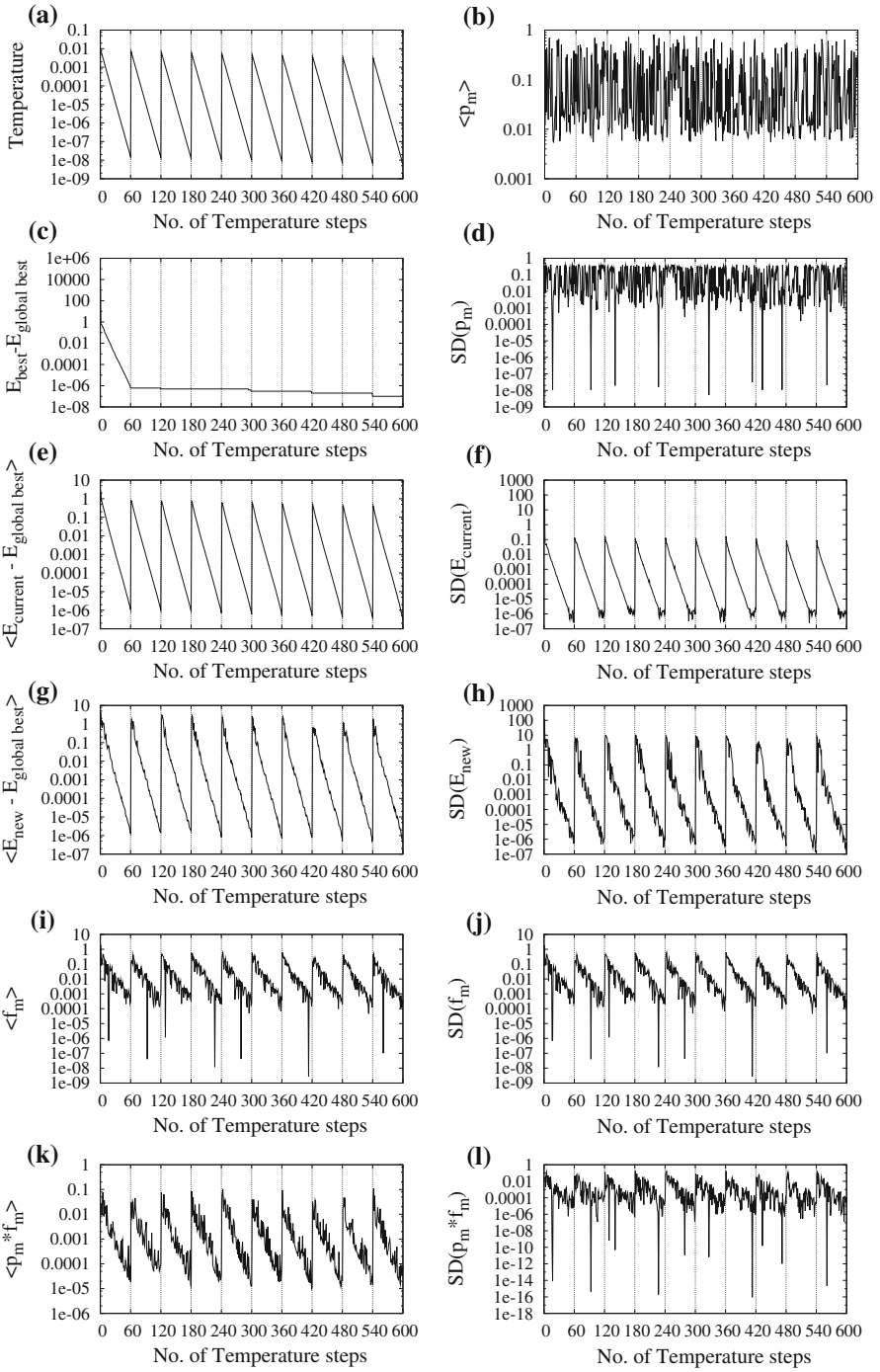

Fig. 8 For standard run ($\lambda_{reheat} = 0.9$, $\lambda_{cool} = 0.8$) with $n_{Metrop} = 1{,}000 * 3n$, adaptive p_m and f_m, $\{x_{current}\}$ reset to $\{x_{best}\}$ after run at a particular $T1$

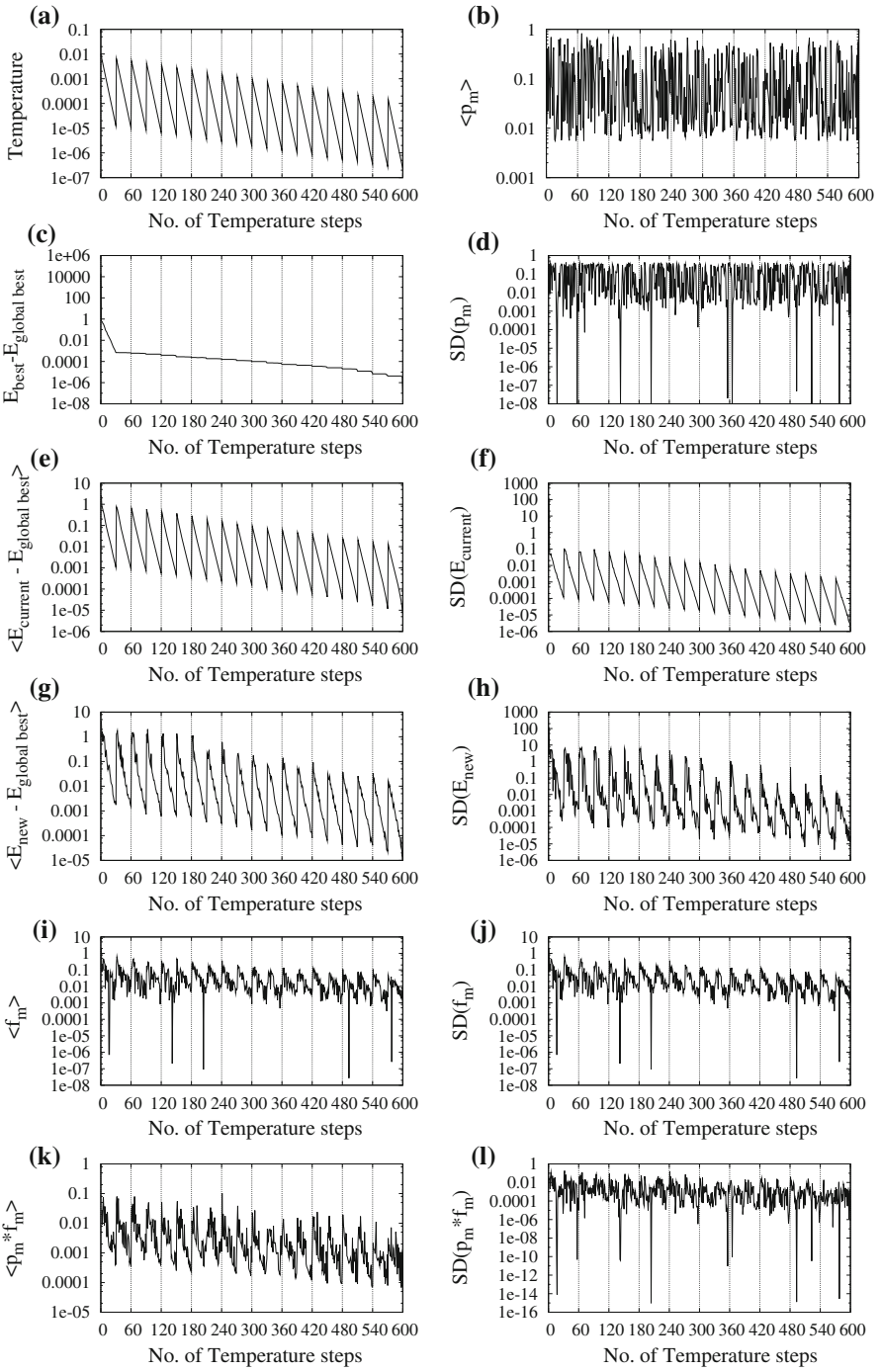

Fig. 9 For standard run ($\lambda_{reheat} = 0.9$, $\lambda_{cool} = 0.8$) with $n_{Metrop} = 1{,}000 * 3n$, adaptive p_m and f_m, $\{x_{current}\}$ reset to $\{x_{best}\}$ after run at a particular T

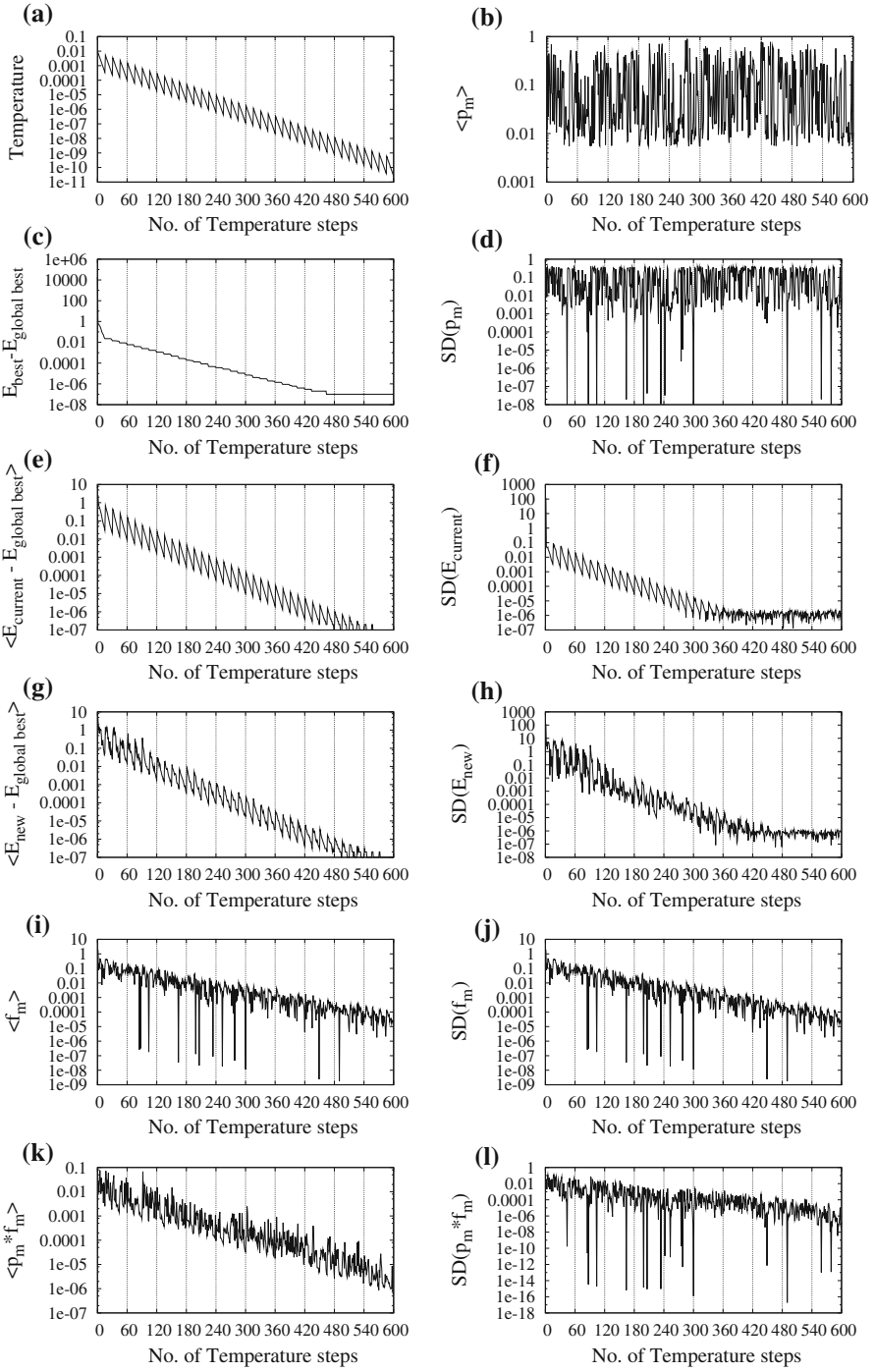

Fig. 10 For standard run ($\lambda_{reheat} = 0.9$, $\lambda_{cool} = 0.8$) with $n_{Metrop} = 1{,}000 * 3n$, adaptive p_m and f_m, $\{x_{current}\}$ reset to $\{x_{best}\}$ after run at a particular T

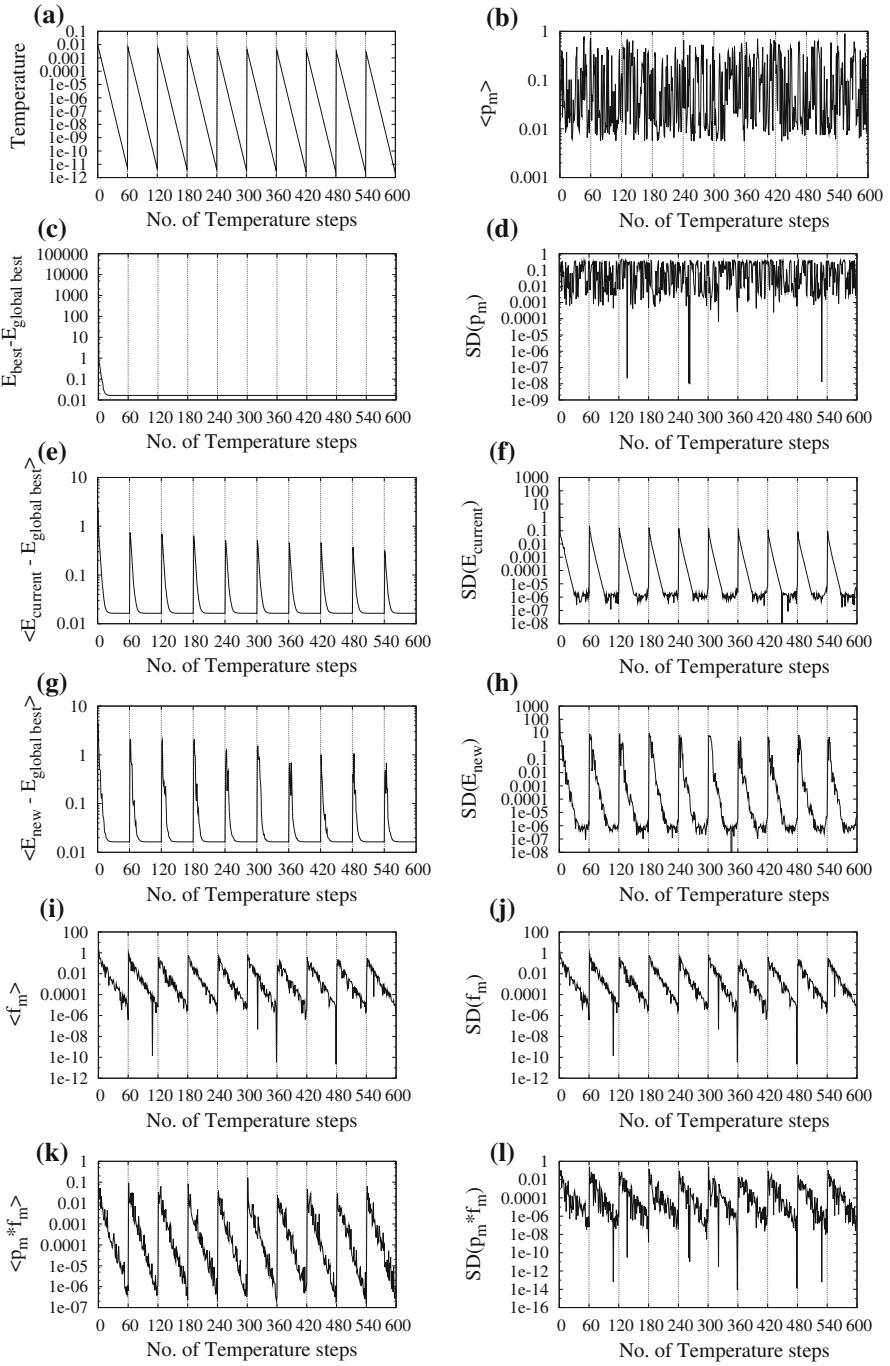

Fig. 11 For standard run ($\lambda_{reheat} = 0.9,\ \lambda_{cool} = 0.7$) with $n_{Metrop} = 1{,}000 * 3n$

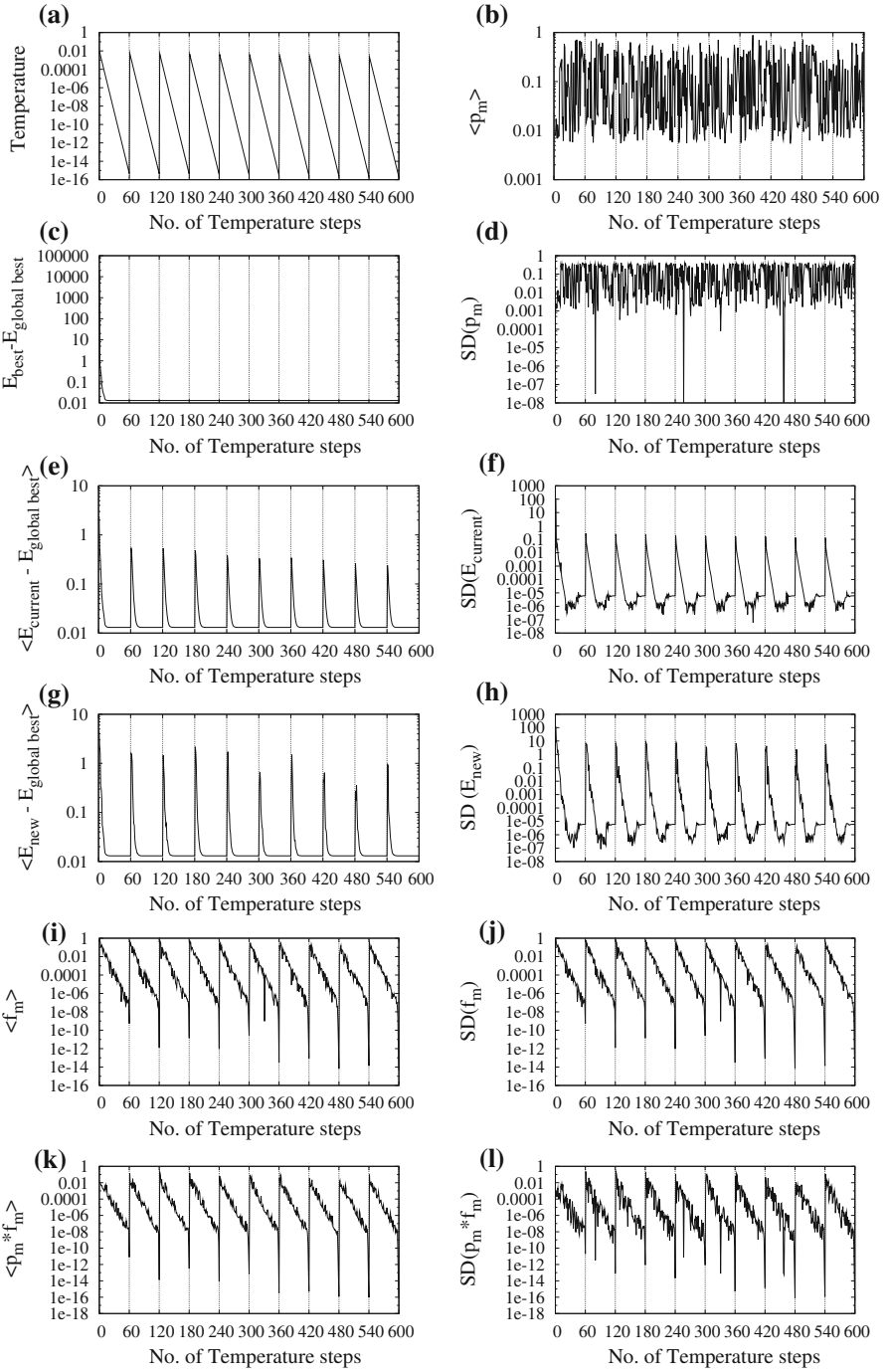

Fig. 12 For standard run ($\lambda_{reheat} = 0.9,\ \lambda_{cool} = 0.6$) with $n_{Metrop} = 1{,}000 * 3n$

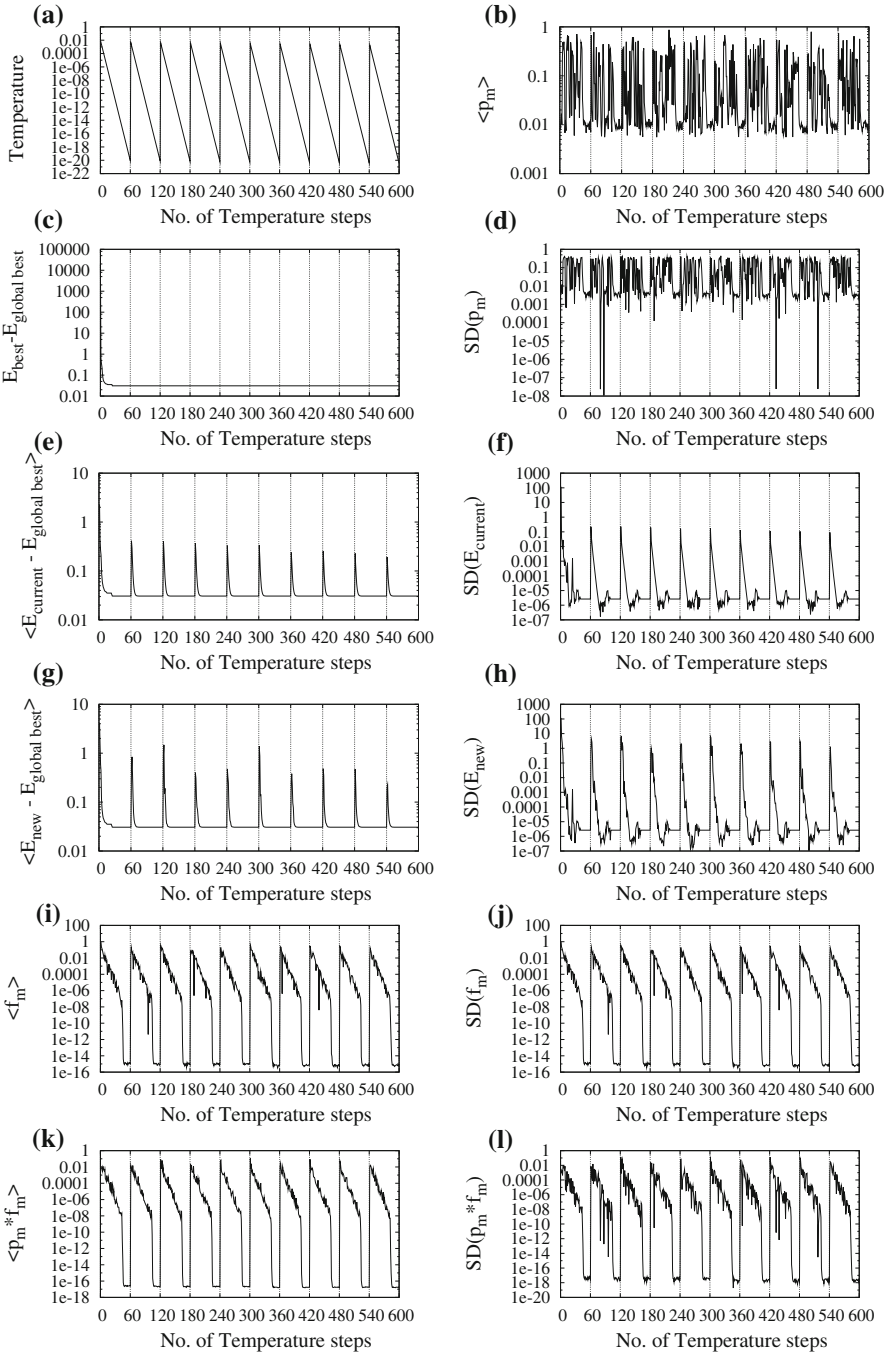

Fig. 13 For standard run ($\lambda_{reheat} = 0.9$, $\lambda_{cool} = 0.5$) with $n_{Metrop} = 1{,}000 * 3n$

Table 2 Comparison of performance of AMSA and SA

AMSA	SA
(i) Global minimum guaranteed for any size	(i) Global minimum not guaranteed
(ii) Global minimum hit in lesser number of temperature steps (∼540)	(ii) Best structure obtained (not necessarily global) takes more steps to reach (∼600 to find a local structure)
(iii) $E_{best} - E_{globalbest} \sim 10^{-6}$	(iii) $E_{best} - E_{globalbest} \sim 10^{-3}$

Table 3 SA parameters used

Number of geometrical parameters	$3N$ where $N = 2 \rightarrow 60$
Allowed range for each geometric parameter	$[x_{min}, x_{max}] = [-20.0, 20.0]$
Initial SA temperature	$T_{in} = 1.0$
Number of cooling steps	$n_{cool} = 60$
Cooling schedule	$T = T_{in} * \lambda_{cool}^{(i_{cool}-1)}$
	$i_{cool} = 1, 2, \ldots, n_{cool}$
Cooling rate	$\lambda_{cool} = 0.8$
Reheating schedule (when 'T' is reset to a high value)	$T_{in}^{new} = T_{in}^{previous} * \lambda_{reheat}$
Reheating rate	$\lambda_{reheat} = 0.9$
Number of Metropolis samples for a particular 'T'	$n_{metrop} = 2,000 * 3N$
Initial mutation probability	$p_m^{initial} = 0.01$
Initial mutation intensity	$f_m^{initial} = 10.0$
Mutation update parameter	$\Delta_y = 0.75$
Adaptive mutation interval	$n_{samples} = \frac{n_{Metrop}}{i_{samples}}$
	$i_{samples} = 4$
Adaptive mutation range $[r_m^{min}, r_m^{max}]$	[0.1, 0.2]

Gupta Potential we have obtained most stable lowest energy isomer. The energies and the point groups of all the stable minima of the three different types of clusters are given in Table 4.

On observation of structure obtained we note that the geometry of the lowest energy structure (stable structure) for a particular nuclearity is strongly dependent upon the composition. Here we have studied the stability of pure Pt, Pd and fifty percent mixed cluster of Pt–Pd alloy. It is important to note that the use of the particular empirical potential neglects the specific electronic effects (e.g. Jahn-teller distortions) which may reverse the ordering of isomer energies leading to the distortion of certain high symmetry structures.

Pt-clusters: Considering the energy values of pure Pt-clusters of different nuclearity in the Table 4 it is clear that a few clusters have relatively much lower energy than the nearest neighbours. The fact is also supported by the more symmetrical point

Table 4 Optimized energy per atom (E) and point group symmetry (PG) parameters of pure Pt, pure Pd and Pt–Pd mixed clusters

Nuclearity (n)	$E\{(Pt)_n\}$	$PG(Pt)$	$E\{(Pd)_n\}$	$PG(Pd)$	$E\{(Pt\text{–}Pd)_n\}$	$PG(Pt\text{–}Pd)$	Nuclearity (n)	$E\{(Pt)_n\}$	$PG(Pt)$	$E\{(Pd)_n\}$	$PG(Pd)$
1					2.8255533	$C_{\infty h}$	31	5.2055534	C_3	3.4219707	C_3
2	3.5339399	$D_{\infty h}$	2.1381417	$D_{\infty h}$	3.6500399	C_{2v}	32	5.2159628	C_3	3.4291757	D_{2d}
3	4.0510936	D_{3h}	2.5205891	C_{3h}	3.9377678	C_s	33	5.2210907	C_s	3.4316546	C_2
4	4.3880162	T_d	2.7752796	T_d	4.0896602	C_s	34	5.2257970	C_1	3.4402320	C_2
5	4.5402479	D_{3h}	2.8933832	D_{3h}	4.1770285	C_s	35	5.2304866	C_s	3.4450657	D_3
6	4.6756908	O_h	2.9974578	O_h	4.2403741	C_1	36	5.2411800	C_2	3.4486235	C_2
7	4.7526143	D_{5h}	3.0589523	D_{5h}	4.2846881	C_1	37	5.2443937	C_1	3.4582198	C_{2v}
8	4.7900021	D_{2d}	3.0880042	D_{2d}	4.3195812	C_1	38	5.2538600	C_s	3.4582658	C_s
9	4.8439730	C_{2v}	3.1320480	C_{2v}	4.3532868	C_1	39	5.2586475	D_3	3.4618727	C_1
10	4.8821760	C_{3v}	3.1640175	C_{3v}	4.3734093	C_1	40	5.2647271	D_2	3.4668924	D_2
11	4.9078099	C_{2v}	3.1867676	C_{2v}	4.3976809	C_1	41	5.2627231	C_1	3.4655115	C_1
12	4.9309927	C_{5v}	3.2128254	C_{5v}	4.4086604	C_1	42	5.2645909	C_1	3.4757542	C_s
13	4.9935645	I_h	3.2665075	I_h	4.4203564	C_1	43	5.2780356	C_2	3.4777057	C_1
14	4.9898900	C_{3v}	3.2613278	C_{3v}	4.4349391	C_1	44	5.2752698	C_1	3.4792744	C_1
15	5.0259338	C_{2v}	3.2811865	C_{2v}	4.4497160	C_1	45	5.2737583	C_1	3.4797290	C_1
16	5.0511746	C_s	3.2953501	C_s	4.4590369	C_1	46	5.2843014	C_1	3.4911149	C_s
17	5.0690738	C_{2v}	3.3094205	C_{2v}	4.4696103	C_1	47	5.2893381	C_s	3.4901639	C_1
18	5.0818128	C_s	3.3190805	C_s	4.4850030	C_1	48	5.2933974	C_1	3.4883041	C_3
19	5.0887009	C_{2v}	3.3263084	C_s	4.4934686	C_1	49	5.2917285	C_1	3.4944939	C_2
20	5.0990600	C_s	3.3363083	C_s	4.4946856	C_1	50	5.2935446	C_1	3.4958823	C_1

Table 4 continued

Nuclearity (n)	$E\{(Pt)_n\}$	$PG(Pt)$	$E\{(Pd)_n\}$	$PG(Pd)$	$E\{(Pt\text{–}Pd)_n\}$	$PG(Pt\text{–}Pd)$	Nuclearity (n)	$E\{(Pt)_n\}$	$PG(Pt)$	$E\{(Pd)_n\}$	$PG(Pd)$
21	5.1066205	C_1	3.3458143	C_1	4.5008741	C_1	51	5.3064732	C_1	3.4986515	C_1
22	5.1306700	C_1	3.3625205	C_s	4.5110250	C_1	52	5.3013356	C_1	3.5036113	C_1
23	5.1428234	C_1	3.3710128	D_{3h}	4.5166459	C_1	53	5.3146306	C_1	3.5098737	C_1
24	5.1539555	C_s	3.3774406	C_s	4.5187095	C_1	54	5.3105002	C_1	3.5020086	C_1
25	5.1576306	C_1	3.3803285	C_1	4.5231230	C_1	55	5.3141311	C_1	3.5119566	C_1
26	5.1665985	C_s	3.3885430	C_s	4.5340825	C_1	56	5.3206943	C_1	3.5069837	C_1
27	5.1776954	C_s	3.3976907	C_s	4.5403174	C_1	57	5.3233495	C_1	3.5115343	C_1
28	5.1878183	C_2	3.4066381	C_1	4.5401425	C_1	58	5.3213773	C_1	3.5165256	C_1
29	5.1978017	C_1	3.4124198	C_2	4.5470493	C_1	59	5.3304682	C_1	3.5177210	C_1
30	5.1988433	C_1	3.4158398	C_1	4.5525643	C_1	60	5.3344920	C_1	3.5162349	C_1

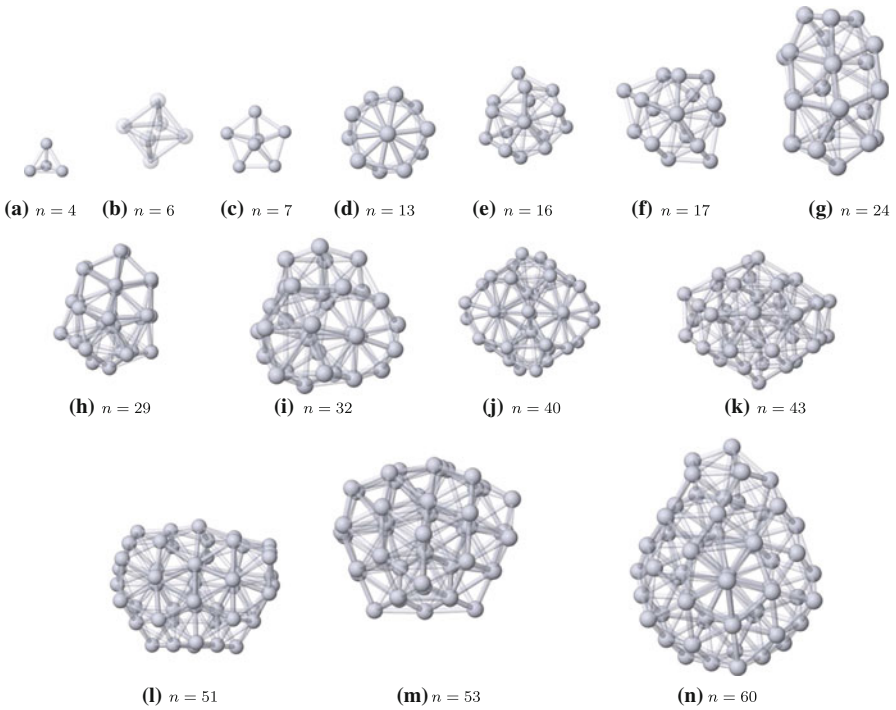

Fig. 14 Structures of stable Pt clusters

groups of the stable clusters [69]. This is also clearly observed when a plot of the difference between E_{fit} and the calculated average binding energy versus nuclearity of cluster is followed (refer to the next section and Fig. 17). Clusters with nuclearity 4, 6, 7, 13, 16, 17, 24, 29, 32, 40, 43, 51, 53, 60 are showing maximum stability (depicted in Fig. 14) where as nuclearity 3, 12, 14, 21 are unstable structures compared to the other Pt-clusters. Sachdev et al. [70] calculated the Pt-cluster structures using many body Embedded atomic Method (EAM) taking icosahedral and cub-octahedral structures and then compared these with structures found by Monte Carlo Simulated Annealing (MCSA). In MCSA search less symmetrical isomers with lower energies are reported to be 'magic numbers' of 13 and 55 atoms. In our discussion 'magic numbers' are 6, 13 with lower nuclearity. Here we have found a number of regular structures along with disorder structures. Again Doye and Wales [74] also found using the Sutton–Chan (SC) many body potential that the icosahedron to be the lowest energy for Pt_{13} cluster.

Pd-clusters: If we look at the nature of the structures of Pd-clusters from our approach we again see the similar geometry of cluster as Pt-clusters mentioned earlier. Using an EAM potential Sachdev et al. [70] found icosahedral global minimum with magic number 13 or 55 atoms of Pd-clusters. Similarly, geometry optimization by Reddy et al. [71] led to the conclusion that the icosahedron is the most stable which was supported by the study using the Corrective Effective Medium (CEM) calculation for $(Pd)_n$ clusters ($n \leq 23$) by Stave and DePristo [72]. These observation have

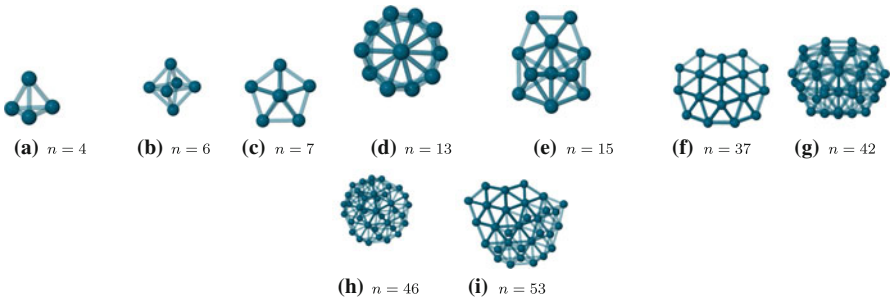

Fig. 15 Structures of stable Pd clusters

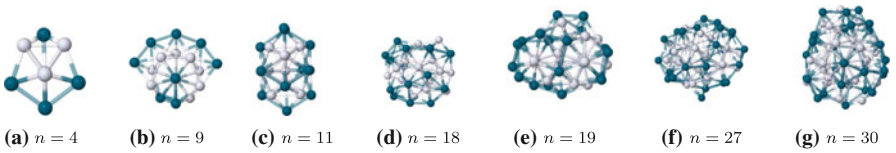

Fig. 16 Structures of stable Pt–Pd clusters (Atoms in dark shade are Pd)

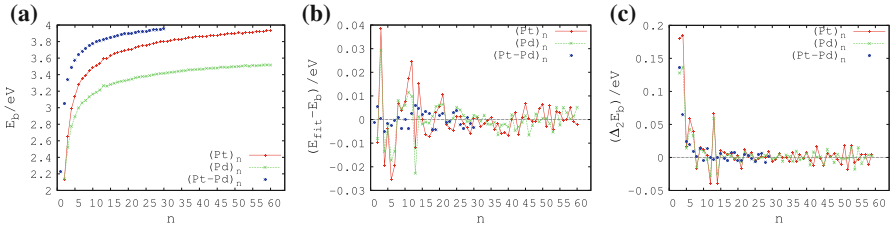

Fig. 17 Plot of **a** Binding Energy E_b (for Pt shifted by 1.4 units and by 0.6 units for mixed Pt–Pd cluster), **b** $(E_{fit} - E_b)$ and **c** $\Delta_2 E_b$, with cluster nuclearity

been supported by the High-resolution electron microscopy studies by Penisson and Renou [73] for Pd-clusters. Again a plot of difference between E_{fit} and E_b versus nuclearity shows particularly stable structures for $n = 4, 6, 7, 13, 15, 37, 42, 46, 53$ (depicted in Fig. 15) and unstable for $n = 3, 11, 21, 25$ Pd-clusters (refer to the next section and Fig. 17). if we observe the plot of the second difference in the binding energies $(\triangle_2 E_b)$ against N, the peaks also support the above stable structures and troughs are the unstable structures.

Pt–Pd-clusters: Due to the low enthalpy of mixing the bulk of Pt–Pd mixed clusters are solid solution. Transmission electron microscopy [75–87] shows the Pt–Pd small clusters to have cub-octahedral structures with fcc packing. Again low energy ion scattering experiments have indicated the surfaces of these Pt–Pd clusters are enriched in Pd rather than homogeneous distribution of Pt and Pd atoms. In stoichiometric $(PtPd)_n$ clusters usually lower cluster $(n \leq 6)$ show icosahedral geometry but larger clusters have distorted geometry. If we see the plot of $(E_{fit} - E_b)$ versus N it is obvious that the range of oscillations in this plot is significantly smaller than previously observed for pure Pt and Pd clusters. There are significant troughs for $n = 4, 9, 11, 18, 19, 27, 30$ (depicted in Fig. 16) showing the stability of clusters

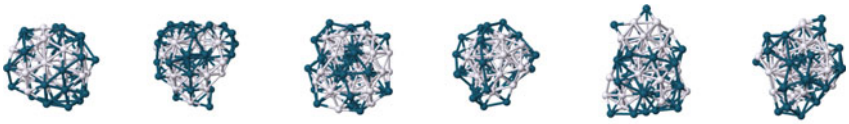

(a) $E = -4.5409092$ **(b)** $E = -4.5127305$ **(c)** $E = -4.5360388$ **(d)** $E = -4.5376387$ **(e)** $E = -4.5190276$ **(f)** $E = -4.5416693$

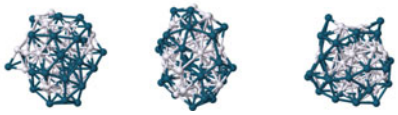

(g) $E = -4.5215249$ **(h)** $E = -4.5318295$ **(i)** $E = -4.5434218$

Fig. 18 Local structures, for a standard run ($\lambda_{reheat} = 0.9$, $\lambda_{cool} = 0.8$) with $n_{Metrop} = 1{,}000 * 3n$ (Atoms in *dark shade* are Pd), for $(Pt–Pd)_{30}$ cluster

and peaks for $n = 2, 13, 25$ showing relatively unstable structure for the particular stoichiometric clusters (refer to the next section and Fig. 17).

In Fig. 18 we have depicted the local structures obtained, for a particular run, after each cooling run in our standard AMSA, without resetting the current co-ordinates to the best so far co-ordinates after each temperature sampling is complete. Thus our method can act as a handy tool to locate not only the global minimum structure but also the low lying and chemically important local minima structures.

3.3 Energetics

The average positive binding energy of N-atom cluster from its total cluster potential energy (V_{clus}) is defined as:

$$E_b = \frac{-V_{clus}}{N} \tag{3.1}$$

Now the second difference of average binding may be represented as:

$$\Delta_2 E_b(N) = 2E_b(N) - E_b(N+1) - E_b(N-1) \tag{3.2}$$

where $\Delta_2 E_b(N)$ denotes the relative stability of an N-atom cluster with respect to its neighbours. Again by fitting the calculated cluster binding energies (E_b) to the following cubic equation in $N^{-\frac{1}{3}}$, we get:

$$E_{fit} = a + bN^{-\frac{1}{3}} + cN^{-\frac{2}{3}} + dN^{-1} \tag{3.3}$$

where a is an estimate of the cohesive energy of the bulk solid, which is obtained from the binding energy of an infinite cluster (as $N \to \infty$). The fitted parameter values for obtaining E_{fit} are depicted in Table 5.

The plots of the above defined quantities against nuclearity, for the three types of clusters considered, have been shown in Fig. 17.

Table 5 Fitted parameter values for obtaining E_{fit}

	Pt	Pd	Pt–Pd
a	6.01648 (6.0412 [20] (5.853 [28])	4.00337 (4.1944 [20]) (3.936 [28])	4.90028 (5.2412 [20]) (4.94 [88])
b	−3.72594	−2.47359	−1.31063
c	5.69845	3.31842	1.36956
d	−6.24932	−4.00108	−2.13485

Data in brackets are from the corresponding references

4 Conclusion

We have shown the efficiency of AMSA as a potent global stochastic optimization scheme by it's application in elucidation of structures of Pt, Pd and Pt–Pd clusters described by the empirical Gupta potential. This potential is extremely rugged and hence is a good case study for testing any optimization scheme. We have further, in detail, tried to explain why the proposed scheme performs much better than conventional Simulated Annealing both in terms of the quality of the solution being found out as also from the point of view of being much more economic in terms of computational time. As a check as to the quality of the metallic clusters being found out we have also tried to find out the specific sizes for which the systems show high stability. Our results are in line with those existing in literature. However, we feel that our proposed method has the ability to handle really tough search surfaces and can be a very handy tool for people needing really good optimization techniques.

Acknowledgments One of us, PC, acknowledges financial support from the Nano-Science Center, University of Calcutta, in the form of a research grant. RS would like to thank the Department of Science and Technology, Government of India, New Delhi, for grant under the FIST program extended to St. Xavier's College, Kolkata.

References

1. R.L. Jonston, *Atomic and Molecular Clusters* (Taylor and Francis, London, 2002)
2. W.B. Pearson, *The Crystal Chemistry and Physics of Metals and Alloys* (Wiley, New York, 1972)
3. J. Jellinek, E.B. Krissinel, in *Theory of Atomic and Molecular Clusters*, ed. byJellinek, (Springer, Berlin, 1999), pp. 277–308
4. H. Yasuda, H. Mori, Phys. Rev. Lett. **69**, 3747 (1992)
5. T. Shibata, B.A. Bunker, Z. Zhang, D. Meisel, C. F. Vademan II, J. D. Gezelter, J. Am. Chem. Soc. **124**, 11989 (2002)
6. J.P. Wilcoxon, P.P. Provencio, J. Am. Chem. Soc. **126**, 6402 (2004)
7. J.L. Rodriguez-Lopez, J. Montejano-Carrizales, U. Pal, J.F. Sanchez-Ramirez, H.E. Troiani, D. Garcia, M. Miki-Yoshida, M. Jose-Yacaman, Phys. Rev. Lett. **92**, 196102 (2004)
8. A.V. Ruban, H.L. Skriver, J.K. Norskov, Phys. Rev. B **59**, 15990 (1999)
9. G. Bozzolo, J. Ferrante, R.D. Noebe, B. Good, F.S. Honecy, P. Abel, Comput. Mater. Sci. **15**, 169 (1999)
10. F. Baletto, C. Mottet, R. Ferrando, Phys. Rev. B **66**, 155420 (2002)
11. A.M. Molenbroek, S. Haukka, B.S. Clausen, J. Phys. Chem. B **102**, 10680 (1998)
12. G. Schmid, in Metal Clusters in Chemistry, vol. 3, eds. by Braunstein, L.A. Oro, P.R. Raithby, (Wiley-VCH, Weinheim, 1999), p. 1325
13. P. Juhas, P.M. Duxbury, W.F. Punch, S.L. Billinge, Nature **440**, 655 (2006)
14. J.O. Joswig, M. Springborg, Phys. Rev. B **68**, 085408 (2003)
15. V.G. Grigoryan, M. Springborg, Chem. Phys. Lett. **375**, 219 (2003)

16. V.G. Grigoryan, M. Springborg, Phys. Rev. B **70**, 205415 (2004)
17. V.G. Grigoryan, D. Alamova, M. Springborg, Phys. Rev. B **73**, 115415 (2006)
18. Y. Dong, M. Springborg, J. Phys. Chem. C **111**, 12528 (2007)
19. X. Shao, X. Liu, W. Cai, J. Chem. Theo. Comput. **1**, 762–68 (2005)
20. C. Massen, T.V. Mortimer-Jones, R.L. Johnston, Dalton Trans. **23**, 4375–4388 (2002)
21. R. Ismail, R.L. Johnston, Phys. Chem. Chem. Phys. **12**, 8607–19 (2010)
22. M.S. Daw, M.J. Baskes, Phys. Rev. B **29**, 6443 (1984)
23. S.M. Foiles, M.J. Baskes, M.S. Daw, Phys. Rev. B **33**, 7983 (1986)
24. A.F. Voter, S.P. Chen, Characterization of defects in materials, in *MRS Symposium Proceedings*, vol. 82, ed. by R.W. Siegal (1987)
25. J.R. Weertman, R. Sinclair (Materials Research Society, Warrendale, PA) p. 175
26. F. Ducastelle, J. Physique **31**, 1055 (1970)
27. R.P. Gupta, Phys. Rev. B **23**, 6265 (1985)
28. F. Cleri, V. Rosato, Phys. Rev. B **48**, 22 (1993)
29. A.P. Sutton, J. Chen, Phil. Mag. Lett. **61**, 139 (1990)
30. J.N. Murrell, R.E. Mottram, Mol. Phys. **69**, 571 (1990)
31. H. Cox, R.L. Johnston, J.N. Murrell, J Solid State Chem. **145**, 571 (1990)
32. J. Rogan, G. Garcia, C. Loyola, W. Orellana, R. Ramirez, M. Kiwi, J. Chem. Phys. **125**, 214708 (2006)
33. J. Rogan, G. Garcia, J.A. Valdivira, W. Orellana, A.H. Romero, R. Ramirez, M. Kiwi, Phys. Rev. B **72**, 115421 (2005)
34. S. Kirkpatric, C.D. Gelatt Jr, M.P. Vecchi, Science **220**, 671–80 (1983)
35. S. Kirkpatric, J. Stat. Phys. **34**, 975–86 (1984)
36. V. Cerny, J. Optim. Theory Appl. **45**, 41–51 (1985)
37. M. Pincus, Oper. Res. **18**, 1225–1228 (1970)
38. D. Vanderbilt, S.G. Louie, J. Comput. Phys. **56**, 259–271 (1984)
39. I.O. Bohachevsky, M.E. Johnson, M.L. Stein, Technometrics **28**, 209–217 (1986)
40. A. Corana, M. Marchesi, C. Martini, S. Ridella, ACM Trans. Math. Softw. **13**, 263–280 (1987)
41. H.H. Szu, in *AIP Conference Proceedings 151* (Snowbird, UT, 1986), pp. 420–425
42. S.K. Biring, P. Chaudhury, Chem. Phys. **377**, 46–53 (2010)
43. S.K. Biring, P. Chaudhury, Chem. Phys. **400**, 198–206 (2012)
44. R. Ahlrichs, S.D. Elliot, Phys. Chem. Chem. Phys. **1**, 13 (1999)
45. J. Holland, *Adaptation in Natural and Artificial Systems* (University of Michigan Press, Ann Arbor, MI, 1975)
46. D.E. Goldberg, *Genetic Algorithms in Search, Optimization and Machine Learning* (Addison-Wesley, Reading, MA, 1989)
47. L. Davis, *Hand Book of Genetic Algorithms* (Van Nostrand Reinhold, New York, 1991)
48. L. Davis, *Genetic Algorithm and Simulated Annealing* (Pitman Publishing, London, 1987)
49. K. Michaelian, N. Rendon, I.L. Garzon, Phys. Rev. B **60**, 2000 (1999)
50. B. Hartke, Angew. Chem. Int. Ed. Engl. **41**, 1468 (2002)
51. R.L. Johnston, Dalton Tran. **22**, 4193–4207 (2003)
52. L.D. Lloyd, R.L. Johnston, S. Salhi, N.T. Wilson, J. Mater. Chem. **14**, 1691 (2004)
53. Z. Li, H.A. Scheraga, Natl. Acad. Sci. USA **84**, 661 (1987)
54. J.P.K. Doye, D.J. Wales, Phys. Rev. Lett. **80**, 1357 (1998)
55. N. Metropolis, A.W. Rosenbluth, M.N. Rosenbluth, A.H. Teller, E. Teller, J. Chem. Phys. **21**, 1087–1092 (1953)
56. S. Geman, D. Geman, IEEE Trans. Pattern Anal. Mach. Int. **6**, 721–741 (1984)
57. A.E.W. Jones, G.W. Forbes, J. Glob. Opt. **6**, 1–37 (1995)
58. N. Azizi, S. Zolfaghari, Comput. Oper. Res. **31**, 2439–2451 (2004)
59. M.T. Vakil-Baghmisheh, A. Navarbaf, in*International Symposium on Telecommunication* (2008), pp. 61–66
60. S. Nandy, R. Sharma, S.P. Bhattacharyya, App. Soft. Comput. **11**, 3946–3961 (2011)
61. K. Sarkar, R. Sharma, S.P. Bhattacharyya, J. Chem. Theor. Commun. **6**, 718–726 (2010)
62. L. Ingber, Math. Comput. Model. **12**, 967–973 (1989)
63. L. Ingber, Math. Comput. Model. **18**, 29–57 (1993)
64. B. Hajek, Math. OR **13**, 311–329 (1988)
65. M.D. Huang, F. Romeo, A. Sangiovanni-Vincentelli, *Proceedings of the IEEE International Conference on Computer Aided Design* (Santa Clara, USA, 1986)

66. J. Thompson, K.A. Dowsland, *Proceedings of the First International Conference on the Practice and Theory of Automated Timetabling* (Napier University, Edinburgh, 1995)
67. K. Dowsland, A. Euro, J. Opt. Res. **68**, 389–399 (1993)
68. H.H. Szu, R. Hartley, Phys. Lett. A **122**, 157–162 (1987)
69. L.O. Paz-Borbon, A. Gupta, R.L. Johnston, J. Mater. Chem. **18**, 4154–4164 (2008)
70. A. Sachdev, R.L. Masel, J.B. Adams, Z. Phys. D **26**, 310 (1993)
71. B.V. Reddy, S.N. Khanna, B.I. Dunlap, Phys. Rev. Lett. **70**, 3323 (1993)
72. M.S. Stave, A.E. DePristo, J. Chem. Phys. **97**, 3386 (1992)
73. J.M. Penisson, A. Renou, J. Cryst. Growth. **102**, 585 (1990)
74. J.P.K. Doye, D.J. Wales, New. J. Chem. **22**, 733–744 (1998)
75. S.H. Yang, D.A. Drabold, J.B. Adams, P. Ordejon, K. Glassford, J. Phys. Cond. Matter **9**, L39 (1997)
76. J. Kua, W.A. Goddard, J. Phys. Chem. B **102**, 9481 (1998)
77. J. Rogan, G. Garcia, M. Ramirez, V. Munoz, J.A. Valdivia, X. Andrada, R. Ramirez, M. Kiwi, Nanotechnology **19**, 205701 (2008)
78. P. Nava, M. Sierka, R. Ahlrichs, Phys. Chem. Chem. Phys. **5**, 3372 (2003)
79. Y. Sun, M. Zhang, R. Foumier, Phys. Rev. B **77**, 075435 (2008)
80. Y. Sun, R. Foumier, M. Zhang, Phys. Rev. A **79**, 043202 (2009)
81. C.M. Chang, M.Y. Chou, Phys. Rev. Lett. **93**, 133401 (2004)
82. L.L. Wang, D.D. Johnson, Phys. Rev. B **75**, 235405 (2007)
83. M. Dessens-Felix, R. Pacheco-Contreras, C. Cruz-Vazquez, A. Posada-Amarillas, A.M. Koster, J. Comput. Theor. Nanosci. **7**, 1–4 (2010)
84. A.J. Renouprez, J.L. Roussel, A.M. Cadrot, Y. Soldo, L. Stievano, J. Alloy Compd. **328**, 50 (2001)
85. J.L. Rousset, L. Stievano, F.J.C.S. Aires, C. Jeantet, A.J. Ronouprez, M. Pellarin, J. Catal. **202**, 163 (2001)
86. I. Efremenko, J. Mol. Catal. **173**, 19 (2001)
87. M. Jose-Yacaman, M. Martin-Almazo, J.A. Ascencio, J. Mol. Catal. A **173**, 61 (2001)
88. E.R. de Boer, R. Boom, W.C.M. Mattens, A.R. Miedeama, A.K. Niessen, *Cohesion in Metals: Transition metal alloys* (Elsevier, Amsterdam, 1988)